THE ASTROPHYSICAL JOURNAL, 455:508–515, 1995 December 20

THE HARD X-RAY EMISSION OF NGC 3628 AND THE CONTRIBUTION OF LOW-LUMINOSITY SPIRAL GALAXIES TO THE COSMIC X-RAY BACKGROUND

TAHIR YAQOOB,[1,2] PETER J. SERLEMITSOS,[1] ANDY PTAK,[1,3] RICHARD MUSHOTZKY,[1]
HIDEYO KUNIEDA,[4] AND YUICHI TERASHIMA[4]

Received 1995 February 24; accepted 1995 June 26

ABSTRACT

We discuss the results of *ASCA* and *ROSAT* observations of the spiral galaxy NGC 3628, which has been previously classified as a starburst. However, X-ray variability establishes the origin of the nuclear emission in a single, compact source, but the luminosity of $\sim 3.4 \times 10^{40}$ ergs s^{-1} is ~ 270 times too large for sub-Eddington accretion onto a 1 $M_\odot$ stellar object. Although the *ASCA* spectrum can be described by a flat power law with a photon index $\Gamma \sim 1.2$, the low statistical quality of the data may conceal a more complex spectrum. However, the *observed* spectrum appears to be much flatter than those of prototypical starburst galaxies, such as NGC 253. The spectrum is harder than Galactic low-mass X-ray binary or black-hole candidate spectra but compatible with high-mass X-ray binary spectra. If the nuclear source is a low-luminosity active galactic nucleus (AGN), the X-ray properties have more in common with Seyfert 1–1.5 galaxies with moderate absorption ($\sim 10^{22}$ cm^{-2}) than with heavily obscured Seyfert 2 galaxies. We also present the first X-ray spectral measurements of the off-nuclear source in NGC 3628 and find it has a steeper spectrum, with $\Gamma > 2.0$ and an *ASCA* luminosity of about half that of the nuclear source. In the light of this and other new *ASCA* observations, we revisit the general problem of the contribution of low-luminosity spiral galaxies to the cosmic X-ray background (CXB) and assess their effect on the parameters of unified AGN models of the CXB as a function of their local luminosity density and X-ray spectral shape.

Subject headings: diffuse radiation — galaxies: individual (NGC 3628) — galaxies: spirial — galaxies: starburst — X-rays: galaxies

1. INTRODUCTION

Prior to *ASCA*, knowledge of the hard (>2 keV) X-ray spectra of low-luminosity ($L_{2-10\,\mathrm{keV}} \sim 10^{40}$ ergs s^{-1}) spiral galaxies had been restricted to a few of the brightest sources (from *EXOSAT*, *Ginga*, and BBXRT; see Petre 1993 and references therein). In general, the X-ray emission was too weak to constrain IPC spectral parameters (Kim, Fabbiano, & Trinchieri 1992). In some cases the nuclear X-ray emission can be confidently attributed to a low-luminosity active galactic nucleus (AGN; e.g., M51, Makishima et al. 1990; M81, Petre et al. 1993; NGC 4258, Makishima et al. 1994). In these cases, the hard X-ray spectrum is often flat, with a power-law photon index $\Gamma \sim 1.4$–1.5 (but for LINER-type objects like M81, $\Gamma \sim 2$). In cases such as the "prototypical starburst galaxies" NGC 253, M82, and M83, the spectra are also steep, with $\Gamma \sim 2$. Although optically thin thermal models are also viable with $kT \sim 6$–7 keV (Ohashi et al. 1990; Ohashi & Tsuru 1992; Petre 1993), the expected iron K-line emission is not detected. The OSSE detection of NGC 253 (Bhattacharya et al. 1994) also argues against thermal emission. The only hard X-ray collective study, based on the summed *HEAO 1* spectra (extending up to ~ 160 keV) of 51 *IRAS*-selected "candidate starbursts," found a flat power-law spectrum with $\Gamma = 1.47 \pm 0.26$ (Rephaeli, Gruber, & Persic 1995). Regardless of their classification as a starburst or AGN, the picture that appears to be emerging is that the hard X-ray emission of low-luminosity spiral galaxies is dominated by one to a few very luminous, often variable, compact sources, *not* by the summed emission from many sources with typical Galactic X-ray binary luminosities ($L_{2-10\,\mathrm{keV}} < \sim 10^{38}$ ergs s^{-1}). For example, the nuclear source in M33 (Takano et al. 1994), "source B" in NGC 1313 (Petre et al. 1994), and "source A" in IC 342 (Okada et al. 1994) all require black holes of greater than 10 $M_\odot$ for sub–Eddington-accretion–driven systems.

Though NGC 3628 is nominally classified as a starburst based on the infrared and radio emission (see Dahlem, Heckman, & Fabbiano 1995 and references therein), the nuclear optical emission is obscured by a dust lane, which conceals the nature of the source. We present the first 0.5–10 keV X-ray spectra of NGC 3628 and address the origin of the X-ray emission and the often-postulated idea that galaxies like NGC 3628 contribute significantly to the cosmic X-ray background (CXB). The structure of the paper is as follows: In § 2 we describe the *ASCA* data and analysis. In § 3.1 we discuss spectral fitting with simple, single-component models, and in § 3.2 more complex models are discussed. In § 3.3 spectral fitting of the off-nuclear source is presented. In § 3.4 we discuss possible origins of the nuclear X-ray emission. In § 4 we revisit the general problem of the contribution of low-luminosity spiral galaxies to the CXB in the light of recent *ASCA* observations. In § 5 we investigate the effects of such a population of galaxies on the parameters of currently popular unified AGN models of the CXB. Our conclusions are summarized in § 6. We use $H_0 = 50$ km s^{-1} Mpc^{-1} and $q_0 = 0$ throughout.

2. *ASCA* DATA

NGC 3628 was observed by *ASCA* on 1993 December 12. (See Tanaka, Inoue, & Holt 1994 for a summary of the *ASCA* mission and focal-plane detectors. Hereafter, the two SIS sensors are referred to as S0 and S1, while the two GIS sensors

[1] Laboratory for High Energy Astrophysics, NASA/Goddard Space Flight Center, Greenbelt, MD 20771.
[2] Universities Space Research Association.
[3] University of Maryland.
[4] Department of Astrophysics, Nagoya University, Chikusa-ku, Nagoya 464-01, Japan.

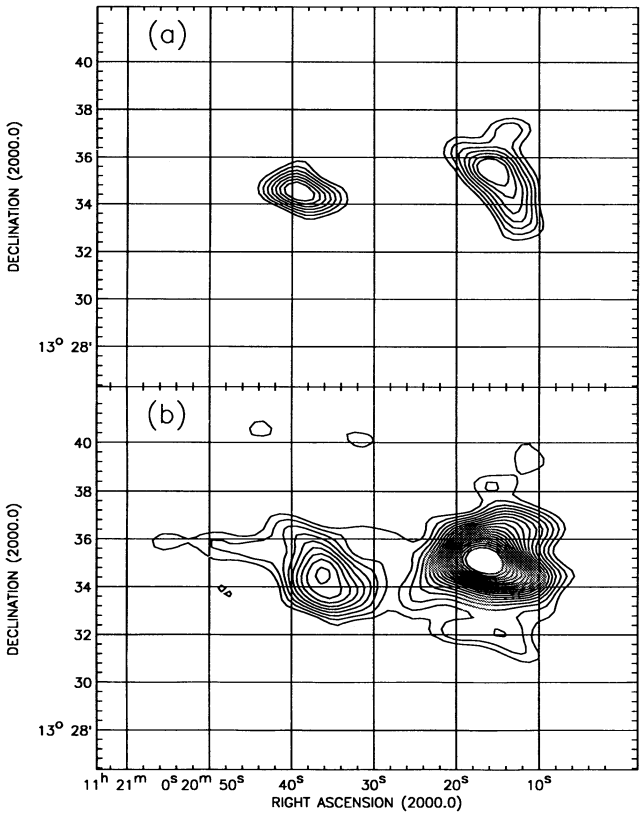

FIG. 1.—*ASCA* S3 image of NGC 3628 (*a*) below 2 keV and (*b*) above 2 keV, smoothed with a $\sigma \sim 30''$ Gaussian (without background subtraction). The contours correspond to levels of 0.45–1.35 smoothed counts at intervals of 0.1 smoothed counts.

are referred to as S2 and S3.) The SIS was in four-CCD mode when the observation was made. The data were cleaned in the manner described in Yaqoob et al. (1994a). Figures 1*a* and 1*b* show the S3 images (with no background subtraction) below and above 2 keV, respectively. The source that lies at the edge of NGC 3628 was first seen by the IPC (Bregman & Glassgold 1982; see also Fabbiano, Heckman, & Keel 1990) and is clearly visible in the GIS data. In S0 the off-nuclear source falls in an interchip gap, and in S1 on a different chip than the nuclear source, which results in insufficient SIS counts for spectral analysis.

Spectra were extracted from 3′ radius circles from all four detectors for the nuclear source and from S2 and S3 for the off-nuclear source. Background spectra were constructed for the SIS from events in the same chip that were far enough away from the point sources and for the GIS from an annulus with radii 8.′8 and 15.′3, centered equidistantly from the two point sources. In the SIS the variation of the internal background with CCD row amounts to $\sim 10\%$ across a chip (Gendreau 1994), and in the GIS the background varies by up to $\sim 20\%$ across the detector (Kubo et al. 1994). Some idea of the systematic effects due to neglect of these spatial variations in the SIS and GIS backgrounds will be given below. Extracted count rates for the nuclear source were in the range 0.9×10^{-2}–1.9×10^{-2} counts s^{-1} for the four instruments, with exposure times $\sim$18–20 ks. The off-nuclear source count rates were $\sim 0.7 \times 10^{-2}$ counts s^{-1} with similar exposure times. The background constitutes $\sim$20%–30% of the total counts. The cross-contamination of the two sources could further complicate the analysis. However, using the convolved XRT + GIS point-spread function (PSF), we estimate that only $\sim 3\%$ of the off-nuclear source counts appear in the 3′ radius nuclear source extraction regions for S2 and S3.

3. SPECTRAL FITS

3.1. *Simple Models*

In the initial spectral analysis of the nuclear source, since it is so weak, we treat the background in two different ways as a consistency check. First (method 1), we model the background spectra from the background regions in each detector (described above) with simple power laws and Gaussians (as required). Method 1 allows the use of the maximum-likelihood statistic for spectral fitting. Second (method 2), we bin the data from the source region to have a minimum of 20 counts per channel (which allows the use of the χ^2 statistic), subtracting the background directly. Using both methods, we fit a simple power-law–plus–absorber model to each instrument individually; the results are shown in Table 1. Unless otherwise stated, all spectral fits refer to SIS data in the 0.5–10 keV range and GIS data in the 0.8–10 keV range. The SIS spectra are likely to contain a greater contribution from the soft extended emission

TABLE 1

SPECTRAL-FITTING RESULTS FOR THE NUCLEAR SOURCE IN NGC 3628[a]

Detector	Method	Γ	N_H (10^{21} cm^{-2})	C/χ^2 [b]
S0	1	0.85 (0.61–1.18)	0.0 (0.0–1.7)	838.0 (342)
S0	2	0.87 (0.61–1.26)	0.2 (0.0–2.7)	21.7 (19)
S1	1	1.02 (0.75–1.47)	0.3 (0.0–3.2)	836.9 (363)
S1	2	0.99 (0.74–1.46)	0.1 (0.0–3.4)	19.2 (20)
S2	1	1.83 (1.12–2.70)	9.3 (0.8–22.2)	974.8 (777)
S2	2	1.89 (1.20–2.84)	9.9 (1.3–15.4)	6.5 (10)
S3	1	1.37 (0.88–2.02)	3.1 (0.0–11.5)	1129.0 (776)
S3	2	1.48 (0.89–2.27)	4.6 (0.0–15.4)	13.0 (14)
S0, S1	2	0.93 (0.74–1.22)	0.2 (0.0–2.0)	41.5 (40)
S0, S1 (>1 keV)	2	1.20 (0.79–1.67)	3.5 (0.0–8.2)	29.0 (33)
S2, S1	2	1.66 (1.20–2.26)	6.9 (1.3–15.1)	19.0 (25)
S0–S3	2	1.16 (0.95–1.40)	1.2 (0.0–3.1)	68.2 (67)

[a] Value ranges in parentheses indicate 90% confidence ranges for two interesting parameters. Method 1 refers to spectral fitting using the maximum-likelihood statistic (C), with the background modeled by simple functions. Method 2 refers to use of χ^2 with the background subtracted directly. See § 3.1 for details.

[b] Values in parentheses are degrees of freedom.

component seen in the *ROSAT* HRI (Dahlem et al. 1995) and the IPC (Fabbiano et al. 1990). Correction for such a component would make the nuclear emission flatter and/or more absorbed. The narrower PSF for the SIS also means there is less cross-contamination from the off-nuclear source. Another important point is that the GIS is not sensitive to columns of the order of $\sim 10^{21}$ cm^{-2} or less.

Table 1 shows that methods 1 and 2 yield entirely consistent results. Unless stated otherwise, all errors refer to 90% confidence for two parameters. The SIS spectral fits give $\Gamma \sim 0.85$–1.0 and a column density N_H comparable to the Galactic value of 1.98×10^{20} cm^{-2} (Hartmann & Burton 1995). The GIS fits give steeper slopes and correspondingly larger columns. Examining the effect of under- or overestimating the background, we find that by artificially decreasing the SIS and GIS backgrounds by 10% and 20%, respectively (see § 2), the SIS slope can be less by up to 0.03 and the GIS slope by up to 0.12. Increasing the SIS and GIS backgrounds by 10% and 20%, respectively, we find the SIS slope changes by only ~ 0.01 while the GIS slope increases by up to ~ 0.10.

The apparent differences in best-fit SIS and GIS parameters in Table 1 are *not* due to cross-calibration systematics between the spectrometers. The agreement between the SIS and the GIS is usually better than 0.05 in the slopes of power-law spectra (see, e.g., Yaqoob et al. 1994a, b). What is more important for a source as weak as this is that the SIS is most sensitive at low energies (below ~ 3 keV), while the GIS is better at high energies. The SIS is thus a much better indicator of the absorbing column than the GIS. However, since N_H and Γ are correlated parameters, the most reliable measure of the overall spectrum should be obtained from simultaneously fitting SIS and GIS data because the GIS data are forced to comply with N_H values consistent with the SIS data (the GIS data alone give a reduced $\chi^2 < 1.0$ even if $N_H = 0.0$). The results of such a four-instrument fit (shown in Table 1 and Figs. 2 and 3) are $\Gamma = 1.16^{+0.24}_{-0.21}$ and $N_H = 1.2^{+1.9}_{-1.2} \times 10^{21}$ cm^{-2}, and this gives a good overall *empirical* description of the data. Note that if the spectrum is really more complex than a power law, the apparent differences in spectral parameters from fitting SIS and GIS separately will be enhanced. We illustrate this by fitting the S0 and S1 data above 1 keV only, with the simple power-law–plus–absorber model, and comparing directly to the same model fitted to S2 and S3 (see Table 1). It can be seen that the SIS data fitted above 1 keV give a best-fit slope that is steeper by ~ 0.3 than that obtained from fitting the data in the full bandpass. The possibility that the true spectrum is more complex than a power law will be discussed below.

From the four-instrument, power-law–plus–absorber fit described above and in Table 1 we obtain mean observed fluxes in the 0.5–2 and 2–10 keV bands of 1.7×10^{-13} and 8.5×10^{-13} ergs cm^{-2} s^{-1}, respectively. Individual values from the four instruments differ by no more than $\pm 25\%$ from the means. The differences represent systematic limitations of absolute flux measurements for sources as weak as this ($\pm 10\%$–20% is more typical of brighter sources). For $D = 14.9$ Mpc (Soifer et al. 1987), the mean absorption-corrected 0.5–2 keV and 2–10 keV luminosities are 0.45×10^{40} and 2.9×10^{40} ergs s^{-1}, respectively.

Note that the overall spectrum is so remarkably flat that, even with so few photons, a single-component thermal model for the continuum can be rejected. Spectral fits to the SIS data with either a thermal bremsstrahlung or Raymond-Smith model push the temperature up to ~ 100 keV. For the bremsstrahlung model, fixing $kT = 10$ keV (the upper end of the *ASCA* bandpass) gives $\chi^2 = 62.3$ (41 degrees of freedom), which rejects the model with greater than 98% confidence. We have also searched for iron K-line emission; fits to S0 and S1 with a power-law continuum (method 1) give an equivalent width of 18^{+292}_{-18} eV (90% confidence, 1 parameter) for a 6.4 keV narrow line ($\sigma = 0.01$ keV). The line is not statistically significant and is omitted in subsequent fits, which use S0–S3 and method 2.

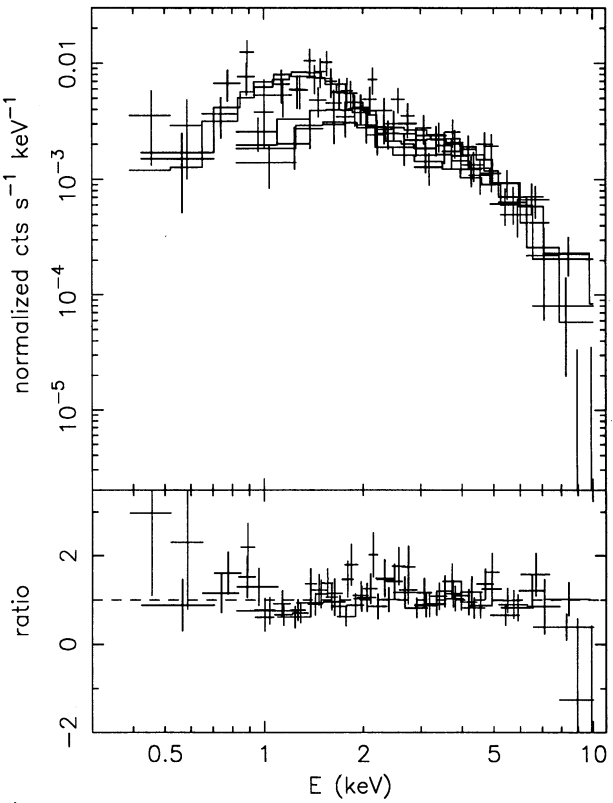

FIG. 2.—*ASCA* four-instrument spectral fit to the nuclear X-ray source in NGC 3628. Shown are the data, best-fit simple power-law–plus–absorber model, and the ratio of data to model.

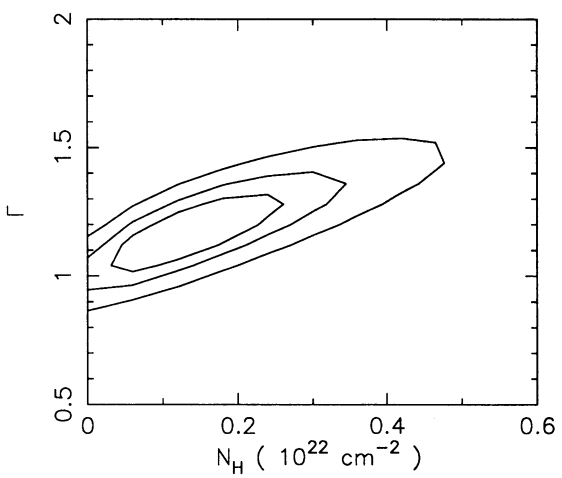

FIG. 3.—Confidence contours of photon index (Γ) vs. column density (N_H) for the four-instrument spectral fit with a simple power-law–plus–absorber model. The confidence levels are 68%, 90%, and 99% for two interesting parameters.

3.2. *Complex Models*

We have also tried complex models. Although the data do not formally require more complexity, this is useful for interpretation of the X-ray emission, provided that the number of free parameters is restricted. First, we fitted an intrinsic continuum consisting of a power law with a high-energy cutoff, $E^{-\Gamma}\exp(-E/E_f)$. An acceptable fit is obtained with $\Gamma = 0.39^{+0.51}_{-0.58}$ and $E_f = 4.3^{+13.5}_{-2.0}$ keV (see Table 2). N_H was fixed to the Galactic value since it tends to zero if it is free. This is an empirical model that describes a spectrum that gradually becomes steeper with increasing energy and has been found to provide a better fit to the nuclear source in M33 than a simple power law (the statistics in that case are much better than for NGC 3628). Given the likelihood of the presence of more than one emission component, this is again more of an empirical description of the data. We stress that the *ASCA* data cannot distinguish between the power-law and cutoff power-law models, but the extrapolations of the two models beyond 10 keV are significantly different.

Next, we asked whether the data are compatible with a power law having a photon index more typical of Seyfert galaxies (Γ fixed at 1.7) that is partially absorbed (i.e., a partial-covering model). The unabsorbed part may correspond to a continuum that is scattered into the line of sight in an extended region. Such a spectrum is typical of Seyfert 2 galaxies (see, e.g., Iwasawa et al. 1994). A good fit is obtained (see Table 2) with $N_H = 17^{+11}_{-7} \times 10^{21}$ cm^{-2} and a covering fraction of 0.72 ± 0.09. We also tried a model with a $\Gamma = 1.7$, fully absorbed power law plus an optically thin thermal component subjected only to Galactic absorption (power law + Raymond-Smith model in Table 2). We obtained a temperature for the thermal component of $kT = 0.67^{+0.16}_{-0.39}$ keV and $N_H = 9.7^{+3.2}_{-2.7} \times 10^{21}$ cm^{-2}.

Finally, as a direct empirical comparison with Galactic low-mass X-ray binaries (LMXBs) and black-hole candidates (BHCs), we fit the data with a multicolor-disk model (MCD; see Mitsuda et al. 1984), characterized by the parameter T_{in} (related to the inner disk temperature). Galactic LMXBs are found to have $T_{in} \sim 1$–1.5 keV, and BHCs have lower values (see Yaqoob, Ebisawa, & Mitsuda 1993). An additional power-law component with $\Gamma \sim 1.6$–2 is common in both types of source. For the NGC 3628 nuclear source, we obtained a harder spectrum than is typical for Galactic LMXBs and BHCs, $T_{in} = 2.9^{+1.1}_{-0.6}$ keV (see Table 2), and inclusion of an additional power law with $\Gamma > 1.6$ increases T_{in} further. Inclusion of an additional soft, optically thin thermal component also increases T_{in}.

TABLE 2

SPECTRAL-FITTING RESULTS WITH COMPLEX MODELS

Model[a]	Parameter	Fitted Value
Cutoff power law	Γ	$0.39^{+0.51}_{-0.58}$
	E_f (keV)	$4.3^{+13.5}_{-2.0}$
	χ^2 (dof)	61.9 (67)
Partial covering	N_H (10^{21} cm^{-2})	17^{+11}_{-7}
	Γ	1.7 (f)
	C_f	0.72 ± 0.09
	χ^2 (dof)	59.1 (67)
Power law + Raymond-Smith	N_H (10^{21} cm^{-2})	10 ± 3
	Γ	1.7 (f)
	kT (keV)	$0.67^{+0.16}_{-0.39}$
	χ^2 (dof)	55.9 (66)
Multicolor disk	kT_{in} (keV)	$2.9^{+1.1}_{-0.6}$
	$r_{in}(\cos\theta)^{0.5}$	0.7[b]
	χ^2 (dof)	61.9 (68)

[a] See § 3.2 for descriptions of models. All errors correspond to 90% confidence for two interesting parameters. When N_H is not given, it has been fixed at the Galactic value of 1.98×10^{20} cm^{-2}. Other parameters that are fixed in the spectral fitting are indicated by (f).

[b] Since the parameter $r_{in}(\cos\theta)^{0.5}$ is related to the model normalization, its uncertainty is dominated by the systematic uncertainty in measuring absolute fluxes (i.e., ~25%).

3.3. *Off-nuclear Source*

The S2 and S3 data from the off-nuclear source are well fitted simultaneously (method 2) with a simple power-law–plus–absorber model, with $\Gamma = 2.39^{+0.91}_{-0.69}$, $N_H = 7.4^{+9.4}_{-6.4} \times 10^{21}$ cm^{-2}, and $\chi^2 = 18.0$ (19 dof). An optically thin thermal model also provides a good fit to the off-nuclear spectrum, giving $kT = 3.5^{+6.3}_{-1.8}$ keV, $N_H = 4.6^{+6.7}_{-4.6} \times 10^{21}$ cm^{-2}, and $\chi^2 = 17.6$ (19 dof). From the power-law fit, average S2 and S3 observed fluxes in the 0.5–2 and 2–10 keV ranges are 0.9×10^{-13} and 2.5×10^{-13} ergs cm^{-2} s^{-1}, respectively. If the off-nuclear source is associated with the galaxy, then the implied 0.5–2 and 2–10 keV *observed* luminosities are 2.5×10^{39} and 6.5×10^{39} ergs s^{-1}, respectively. This corresponds to 0.5–2 and 2–10 keV absorption-corrected luminosities of 10.7×10^{39} and 7.1×10^{39} ergs s^{-1}, respectively. Archival PSPC data from 1991 November alone are too poor to constrain the spectrum but, fitted simultaneously with S2 and S3 with a power-law–plus–absorber model, give $\Gamma = 2.09^{+0.60}_{-0.47}$, $N_H = 3.9^{+4.0}_{-2.9} \times 10^{21}$ cm^{-2}, and a 0.5–2 keV flux of 0.8×10^{-13} ergs cm^{-2} s^{-1}. Thus, within the uncertainties, there is no evidence that the source varied between the PSPC and *ASCA* observations. The X-ray spectrum is compatible with LMXB spectra or very young supernova remnants (cf. sources in NGC 1313; Petre et al. 1994). However, the intrinsic, albeit model-dependent, 0.5–10 keV luminosity is, like the nuclear source, apparently super-Eddington for a 1 $M_\odot$ stellar object ($\sim 149\ L_{EDD}$).

3.4. *Origin of the Nuclear X-Ray Emission*

The 0.5–2 keV flux of the nuclear source in the 1991 November PSPC observation (6.7×10^{-13} ergs cm^{-2} s^{-1}; see Dahlem et al. 1995 for details) is over a factor of 3 greater than the corresponding *ASCA* flux. This, along with the diminishing of the *ROSAT* HRI flux by a factor of more than 27 between 1991 December and 1994 May, unequivocably establishes that the nuclear X-ray emission originates in a single, compact object. Yet, the luminosity exceeds the Eddington limit by at least 2 orders of magnitude for a 1 $M_\odot$ accretion-driven system. The variability could be intrinsic or due to variable absorption. The X-ray spectrum measured by *ASCA* is compatible with that of a high-mass X-ray binary (HMXB; Nagase 1989) or a moderately absorbed, low-luminosity AGN. In the latter case, $N_H \sim 10^{22}$ cm^{-2} but could have been an order of magnitude higher during the 1994 May HRI observation. This behavior more closely resembles that observed in Seyfert 1–1.5 galaxies exhibiting complex and variable absorption (see, e.g., Warwick et al. 1993) than Seyfert 2 galaxies, which also typically show iron K-line emission with an equivalent width of a few hundred electron volts. Of course, the source may be none of these familiar objects but rather an accreting system that has

a central mass that is intermediate to typical Galactic systems and AGNs.

4. CONTRIBUTION OF LOW-LUMINOSITY SPIRAL GALAXIES TO THE CXB

The *ASCA* spectrum of NGC 3628 is interesting from the point of view that it may be as flat or flatter than the CXB, which can be described adequately by a straight power law in the 1–10 keV band with $\Gamma \sim 1.4$ (Gendreau et al. 1994). Currently, a promising model of the origin of the CXB is that of a combination of Seyfert 1 and Seyfert 2 galaxy populations (e.g., Setti & Woltjer 1989; Madau, Ghisellini, & Fabian 1993, 1994; Matt & Fabian 1994; Comastri et al. 1995), but neither class of source alone has a spectrum that matches the CXB (the "spectral paradox"). Note that the Seyfert 2 galaxies in this picture are very heavily absorbed, with $N_H > 10^{23}$ cm^{-2}. The question naturally arises as to whether NGC 3628 represents a class of source that does not suffer from the spectral paradox and whether such a class could be sufficient in number to make a significant contribution to the CXB. In particular, could NGC 3628 be representative of the new class of hard X-ray sources that have shown up in recent *ROSAT* deep surveys, albeit at a 1–2 keV flux level an order of magnitude below that of NGC 3628 (Hasinger et al. 1993; Jones et al. 1995)? The idea that starburst galaxies (recall that NGC 3628 has been classified previously as one) could be made up of HMXBs with flat hard-X-ray spectra ($\Gamma \sim 1.0$–1.3), thus easing the spectral mismatch with the CXB, is not a new one (e.g., Griffiths & Padovani 1990). However, direct observational evidence to support this has been scarce. Generally, the sources are so weak that, prior to *ASCA*, their hard X-ray spectral parameters could not be constrained (see, e.g., Kim et al. 1992). The few bright ones, like NGC 253, M82, and M83, show instead a fairly steep spectrum ($\Gamma \sim 2$; Ohashi et al. 1990; Ohashi & Tsuru 1992). On the other hand, *ASCA* observations of so-called normal or starburst galaxies so far indicate a variety of hard X-ray slopes in the range ~ 1.4–2.0 (see § 1; see also Makishima 1994 and references therein), and NGC 3628 extends this range down to $\Gamma \sim 1.2$ or less. Since the galaxies observed by *ASCA* so far have not been selected systematically on the basis of any particular criterion, we cannot make a meaningful statement about the distribution in Γ. Thus, in the following, we make the conservative assumption that Γ can be anywhere in the range 1.0–2.0.

Currently popular unified AGN models of the CXB (e.g., Madau et al. 1993, 1994; Matt & Fabian 1994; Comastri et al. 1995) explicitly ignore the contribution from spiral galaxies (often *IRAS*-selected) that have not been identified as Seyfert galaxies (type 1 or 2) or quasars and thus been lumped together as "starbursts" (NGC 3628 is in the latter group). On the other hand, many authors have tried to quantify the "starburst" contribution. Griffiths & Padovani (1990), using both *IRAS* bright-galaxy and optically selected starburst samples, assumed all sources had $\Gamma = 1.3$ and used no observational X-ray information above 3 keV. From *ASCA* observations of some of these sources so far (§ 1), we know this assumption is not correct. On the other hand, Ricker & Mészáros (1993) calculated the CXB contribution based on what starburst X-ray spectra *should* be, assuming compositions of LMXBs and HMXBs, again with no input from hard X-ray observations. Rephaeli et al. (1995) used an average 0.5–160 keV *HEAO 1* spectrum of 51 galaxies. However, the biases of this and other samples (e.g., Griffiths & Padovani 1990) are troublesome. For example, Rephaeli et al. (1995) do not include NGC 3628, yet they include NGC 3147, which is now known to be a low-luminosity AGN (Moran, Halpern, & Helfand 1994; Ptak et al. 1996). Here we reassess the contribution of "low-luminosity non-AGN spirals" (hereafter LLNAS) to the CXB. By LLNAS we mean spiral galaxies with $L_{2-10\,\mathrm{keV}}$ less than $\sim 10^{42}$ ergs s^{-1} that are not classified as Seyfert 1 or Seyfert 2. Misclassifications of objects in previous samples thought to consist of normal/starburst galaxies but that are really AGNs mean that previous estimates of the LLNAS local luminosity density may have been too high. Such objects should instead appear at the lower luminosity end of the AGN luminosity function and thus increase the local luminosity density of AGNs relative to previous estimates. In our estimates we will use extreme values of $\Gamma_{2-10\,\mathrm{keV}}$ of 1.0 and 2.0 (and also appeal to an intermediate value of 1.5). This is more observationally accurate than previous estimates. However, to estimate the CXB contribution at energies greater than 10 keV/$(1 + z_{\max})$ ($z_{\max}$ is the maximum redshift of the sources) requires knowledge of the spectral shape of the LLNAS above 10 keV (i.e., above the *ASCA* bandpass). For this, observational information is very limited. The only information we have is the average 0.5–160 keV spectrum of Rephaeli et al. (1995), with its associated caveats, and the OSSE detection of NGC 253 (Bhattacharya et al. 1994), a prototype starburst. Thus, we take the most general approach and take the slope above 10 keV to be a free parameter. Hereafter, we shall refer to the effective slopes below and above 10 keV as Γ_1 and Γ_2, respectively. For our purpose, this broken power-law spectrum is an adequate empirical description of the spectrum from LMXBs, HMXBs, or AGNs and has the advantage that the CXB contribution can be examined in an analytic form. The X-ray spectra from these three types of sources are more commonly described in terms of a power law with an exponential cutoff of the form $\exp(-E/E_f)$. Typically, for LMXBs and HMXBs, $E_f \sim 5$–20 keV (e.g., Ricker & Mészáros 1993), whereas for AGN-type sources $E_f \sim 100$ keV and up (e.g., Zdziarski et al. 1995). We can find an approximate correspondence to the broken power-law spectrum by joining the 10 keV and $10(1 + z_{\max})$ keV fluxes by a straight line in log-log space, which gives us $\Gamma_2 \sim \Gamma_1 + [10 z_{\max}/E_f \ln(1 + z_{\max})]$. For $z_{\max} = 3$ and $E_f \sim 5$–20 keV, $\Delta\Gamma \equiv \Gamma_2 - \Gamma_1 \sim 4.3$–$1.0$ (LMXBs, HMXBs), and for $E_f > 20$ keV, $\Delta\Gamma < 1.0$ (AGN-like sources).

Now, the percentage contribution to the CXB at an energy E_0 (keV) due to a population of sources with broken–power-law X-ray spectra that is undergoing pure luminosity evolution $\propto (1 + z)^{\gamma}$ (out to $z = z_{\max}$) can be written (see discussion in Boldt 1987)

$$P(E_0, \Gamma_1, \Gamma_2, E_b, z_{\max}, \gamma) = \frac{314.6 \rho_{38} F(E_0, \Gamma_1, \Gamma_2, E_{b,z_{\max}}, \gamma, q_0)}{I_{\mathrm{CXB}}(E_0) \int_{E_1}^{E_2} E^{1-\Gamma_1} dE} \% . \quad (1)$$

The intrinsic source spectrum has power-law photon indices Γ_1 and Γ_2 below and above an energy E_b in the source rest frame. In our formulation of the problem, $E_b = 10$ keV and Γ_1 represents the measurable slopes of the X-ray spectra below 10 keV, while Γ_2 represents the largely unknown slopes of the spectra above 10 keV. The local luminosity density of the sources in the energy band E_1 to E_2 (it is assumed that $E_1 < E_2 < E_b$) is ρ_{38} (10^{38} ergs s^{-1} Mpc^{-3}). For the CXB intensity $I_{\mathrm{CXB}}(E_0)$ keV cm^{-2} s^{-1} sr^{-1} keV^{-1}, we use the functional form given by Gruber (1992). Defining $\beta \equiv \gamma - 1 - q_0$ (q_0 is only

allowed to take the values 0.0 or 0.5; in our case $q_0 = 0.0$) and $z_b \equiv (E_b - E_0)/E_0$, the function F is given by

$$
\begin{aligned}
&F(E_0, \Gamma_1, \Gamma_2, E_b, z_{\max}, \gamma, q_0) \\
&= E_0^{1-\Gamma_1} \int_0^{z_{\max}} (1+z)^{\beta-\Gamma_1}\, dz, \qquad E_0 \le \frac{E_b}{1+z_{\max}}, \\
&\quad E_0^{1-\Gamma_1} \int_0^{z_b} (1+z)^{\beta-\Gamma_1}\, dz \\
&\quad + E_b^{\Gamma_2-\Gamma_1} E_0^{1-\Gamma_2} \int_{z_b}^{z_{\max}} (1+z)^{\beta-\Gamma_2}\, dz, \qquad \frac{E_b}{1+z_{\max}} < E_0 < E_b, \\
&\quad E_b^{\Gamma_2-\Gamma_1} E_0^{1-\Gamma_2} \int_0^{z_{\max}} (1+z)^{\beta-\Gamma_2}\, dz, \qquad E_0 \ge E_b .
\end{aligned}
\tag{2}
$$

We adopt $\gamma = 3.2$ from Saunders et al. (1990), who found $\gamma = 3.2 \pm 1.0$ from an *IRAS*-selected sample of starburst galaxies. The local luminosity density ρ_{38} is not very well known. Ricker & Mészáros (1993) estimated $\rho_{38}(0.5\text{–}4.5\ \text{keV}) = 0.43$ by integrating an X-ray luminosity function derived from a correlation of 60 μm and X-ray luminosities of *IRAS* bright galaxies. The mean X-ray spectrum and number density of the Rephaeli et al. (1995) bright-galaxy sample give $\rho_{38}(0.5\text{–}4.5\ \text{keV}) = 0.51$. Miyaji et al. (1994) derive, from an *IRAS* galaxy–CXB cross-correlation analysis, an upper limit on the "non-AGN" value of $\rho_{38}(2\text{–}10\ \text{keV})$ of ~ 2. For $\Gamma = 1.4$, $\rho_{38}(0.5\text{–}4.5\ \text{keV}) = 0.73\rho_{38}(2\text{–}10\ \text{keV})$, so this upper limit corresponds to $\rho_{38}(0.5\text{–}4.5\ \text{keV}) < 1.5$. In Figure 4 we show P at 2 keV (*dotted curves*) for $z_{\max} = 1$ and 3 as a function of Γ, where $\Gamma_1 = \Gamma$ since the CXB contribution at 2 keV depends only on the spectrum up to rest-frame energies of $2(1 + z_{\max})$ keV. All the curves in Figure 4 have been normalized to $\rho_{38}(0.5\text{–}4.5\ \text{keV}) = 0.50$. The dashed curves in Figure 4 show P at 10 keV (for $z_{\max} = 1$ and 3) as a function of Γ, where now $\Gamma_2 = \Gamma$ and $\Gamma_1 = \min(2.0, \Gamma)$. The solid curves in Figure 4 use the same parameters except that $\Gamma_1 = \min(1.0, \Gamma)$. Thus, we cover the observed range in power-law slopes below 10 keV of $\sim 1\text{–}2$.

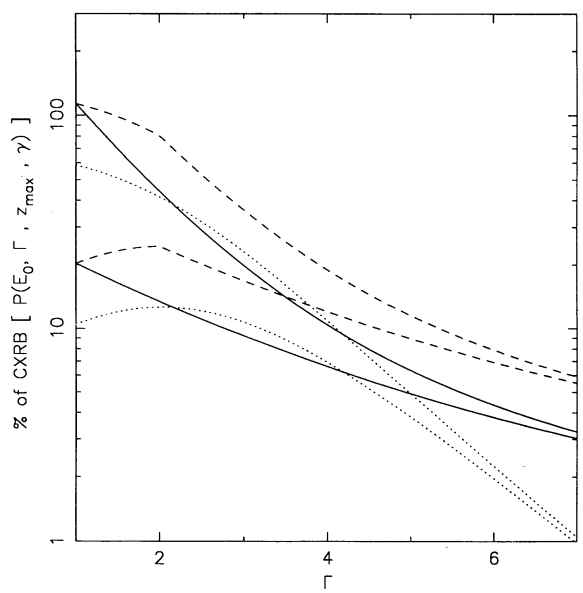

FIG. 4.—Percentage contribution P to the CXB of sources with power-law X-ray spectra with photon indices Γ_1 and Γ_2 below and above 10 keV, respectively (see § 4 for details). The sources undergo pure luminosity evolution of the form $(1 + z)^{\gamma}$, with $\gamma = 3.2$. Shown are P at 2 keV with $\Gamma_1 = \Gamma$ (*dotted curves*), P at 10 keV with $\Gamma_1 = \min(2.0, \Gamma)$ and $\Gamma_2 = \Gamma$ (*dashed curves*), and P at 10 keV with $\Gamma_1 = \min(1.0, \Gamma)$ and $\Gamma_2 = \Gamma$ (*solid curves*). In each case the lower and upper curves correspond to $z_{\max} = 1$ and 3, respectively. All curves are normalized to $\rho_{38}(0.5\text{–}4.5\ \text{keV}) = 0.50$.

Figure 4 shows that the CXB contribution at 2 keV for $z_{\max} = 3$ is as high as $58(\rho_{38}/0.5)\%$ and $41(\rho_{38}/0.5)\%$ for $\Gamma_1 = 1.0$ and 2.0, respectively. These are comparable to previous estimates. Since the CXB contribution at 2 keV depends only on the spectral shape up to energies for which we have solid observational information, the largest uncertainty is in ρ_{38}. The contribution at 10 keV, though, depends crucially on Γ_2. If the source spectra extend to $\sim 40\text{–}50$ keV in the rest frame without a significant steepening (e.g., AGN-like sources), then they could easily dominate and even overpredict the CXB at 10 keV. If the emission is due to LMXBs, HMXBs, or low-temperature thermal sources ($\Gamma_2 > 2$), then P at 10 keV is no more than a few percent. In the latter case, the sources may still have a significant impact on understanding the CXB spectrum because the differential contributions at 2 and 10 keV mean that the shape of the residual CXB that is to be explained (e.g., by AGN models) may be very different from that observed.

5. EFFECTS ON THE PARAMETERS OF UNIFIED AGN MODELS OF THE CXB

Unified AGN models of the CXB consist of a population of Seyfert 1 galaxies and quasars represented by unabsorbed power-law spectra plus Seyfert 2 galaxies represented by absorbed power-law spectra (e.g., Matt & Fabian 1994; Madau et al. 1993, 1994; Comastri et al. 1995). In the simplest versions of these models, the distributions of the power-law spectral indices and absorbing columns are taken to be single-valued, adjustable parameters, and the luminosity function and evolution of Seyfert 1 galaxies and quasars (determined from *ROSAT* deep surveys; e.g., Boyle et al. 1993, 1994) are assumed to be the same for Seyfert 2 galaxies. These models are highly successful in explaining the overall shape of the CXB, in particular the broad hump peaking at ~ 30 keV. However, they explicitly ignore the CXB contribution of LLNAS, and in this section we wish to investigate the qualitative effects on the inferred AGN-model parameters when LLNAS are not ignored. Specifically, we examine the CXB in the 1–10 keV band since Gendreau et al. (1994) have demonstrated that, in this band, a single power law with $\Gamma = 1.4$ provides an excellent description of the CXB, with deviations not larger than systematic errors. Since our purpose is only to investigate the sensitivity of inferred AGN-model parameters to the LLNAS component, we will make several simplifying assumptions. Our method will be to select baseline AGN and LLNAS models and then investigate the effects of deviations from them. As our baseline AGN model, we assume $z_{\max} = 3$ and a luminosity-evolution index $\gamma_{\rm AGN}$ (see § 4) of 2.75, values consistent with the results of Boyle et al. (1993, 1994). We assume $\Gamma_{\rm AGN} = 1.7$ [no exponential cutoff since we are only considering energies up to $10(1 + z_{\max})$ keV] and the absence of any Compton reflection component (see Zdziarski et al. 1995). A fraction f of the primary power law is absorbed by a column density $N_{\rm H}$. We ignore Compton scattering in the absorbing medium. The parameter f is only approximately the fraction of the number of Seyfert 2 galaxies relative to the total AGN number because a few percent of the flux in individual Seyfert 2 galaxies is unabsorbed (Iwasawa et al. 1994). For our baseline LLNAS model, we assume a power law below 10 keV with $\Gamma = 1.5$ (intermediate between 1.0 and 2.0; see § 4). Above 10 keV we assume

representative values of Γ_2 of 1.5, 2.5, and 5.5 (i.e., $\Delta\Gamma = 0.0$, 1.0, and 4.0). We performed our calculations for the range in the LLNAS ρ_{38}(2–10 keV) allowed for the non-AGN contribution to the CXB (i.e., 0.0–2.0; Miyaji et al. 1994). Our main objective is to investigate the effect of ρ_{38} and $\Delta\Gamma$ (i.e., the spectral shape of LLNAS above 10 keV) on N_H and f. We then proceeded to find the best-fitting parameters of the above AGN-plus-LLNAS CXB model that give the best approximation to the $\Gamma = 1.4$ power law describing the CXB (Gendreau et al. 1994). This was done by simulating *ASCA* data using an exposure time of 10^7 s. In the following, statistically acceptable fits were obtained except where stated (this provided additional constraints). Figure 5 shows the resultant best-fit values of N_H and f as a function of ρ_{38}(2–10 keV) for $\Delta\Gamma = 0.0$, 1.0, and 4.0. It can be seen that with no LLNAS contribution, $N_H \sim 4 \times 10^{23}$ cm^{-2} and $f \sim 0.45$. Note that the ratio of Seyfert 2 to Seyfert 1 galaxies in this context does not have a firm observational constraint because different methods of selection give different ratios; it also is not obvious whether the Seyfert 2 galaxies that contribute to the CXB are necessarily those that we observe individually. For the single power-law LLNAS spectrum ($\Delta\Gamma = 0.0$, *dashed curves*), increasing ρ_{38}(2–10 keV) has litle effect on N_H, but f eventually rises to 1.0 near ρ_{38}(2–10 keV) = 2.0. Since the LLNAS represent an unabsorbed population, f increases to compensate for the increase in ρ_{38}(2–10 keV). However, if the LLNAS spectrum drops off steeply above 10 keV (e.g., $\Delta\Gamma = 1.0$ and 4.0, *solid curves* and *dotted curves*, respectively), N_H also increases with ρ_{38}(2–10 keV) (by more than a factor of 3) because the high-energy cutoff in the LLNAS spectrum and the low-energy cutoff in the AGN spectrum compensate for each other. It is interesting to note that the simple condition that at least some unabsorbed AGNs contribute to the CXB implies an upper limit on ρ_{38}(2–10 keV), which for this simple model is ~ 2 regardless of $\Delta\Gamma$ and happens to be coincident with the Miyaji et al. (1994) value obtained by completely independent means.

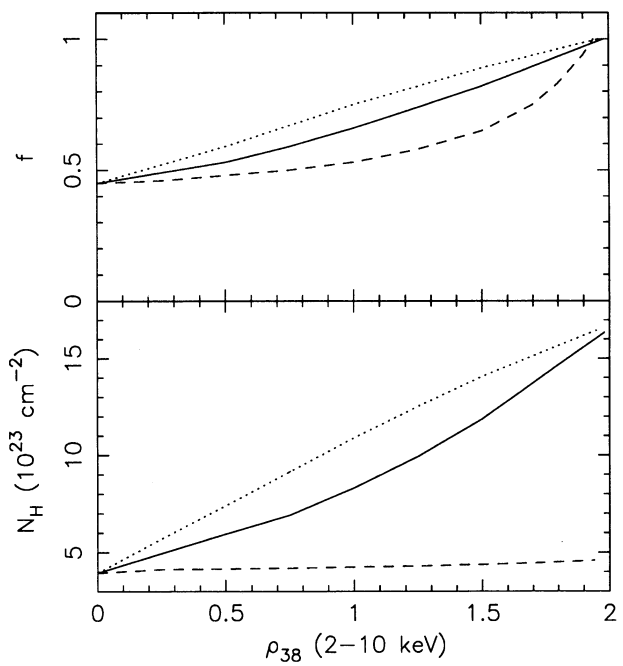

FIG. 5.—Effect on the two key parameters, N_H and f, of a simple unified AGN model of the CXB as a function of the local luminosity density (ρ_{38}) and X-ray spectral shape of a population of low-luminosity spiral galaxies. In the AGN model, a fraction f of the total AGN emission is absorbed by a column density N_H. See § 5 for details of the other parameters of the AGN model. The low-luminosity galaxy spectra have power-law photon indices of 1.5 below 10 keV and are integrated out to $z_{max} = 3$. The dashed curves show the behavior of N_H and f if this power law extends out to $10(1 + z_{max})$ keV without a break. The solid and dotted curves correspond to cases in which the spectrum steepens above 10 keV by $\Delta\Gamma = 1.0$ and 4.0, respectively.

Finally, we examined the effect of altering the baseline LLNAS-plus-AGN CXB spectrum can no longer be approximated by the $\Gamma = 1.4$ power law. With acceptable values of ρ_{38}, the effect of increasing the LLNAS Γ_1 from 1.5 to 2.0 is to increase f by $\sim 10\%$ (steeper LLNAS contribution requires more absorbed AGNs), while N_H can decrease by up to a factor of ~ 2. Naturally, when Γ_1 is decreased from 1.5 to 1.0, N_H and f show the opposite behavior, with similar fractional changes.
ing N_H) and is larger (thus affecting f). If we set the LLNAS Γ_1 to the extreme values 1.0 and 2.0, increasing ρ_{38} beyond ~ 0.5–1.0 (exact value depending on other parameters), the combined LLNAS-plus-AGN CXB spectrum can no longer be approximated by the $\Gamma = 1.4$ power law. With acceptable values of ρ_{38}, the effect of increasing the LLNAS Γ_1 from 1.5 to 2.0 is to increase f by $\sim 10\%$ (steeper LLNAS contribution requires more absorbed AGNs), while N_H can decrease by up to a factor of ~ 2. Naturally, when Γ_1 is decreased from 1.5 to 1.0, N_H and f show the opposite behavior, with similar fractional changes.

6. CONCLUSIONS

An *ASCA* observation of NGC 3628 reveals an X-ray power-law spectrum with a photon index of ~ 1.2, one of the flattest measured for spiral galaxies that are ordinarily classified as normal or starburst (or simply non-AGN). We have qualitatively assessed the impact of these LLNAS (low-luminosity non-AGN spirals) on unified AGN models of the CXB as a function of their local luminosity density and their spectral shape. We find that if the LLNAS spectra cut off sharply above 10 keV, as would be expected if the emission were due to LMXBs, HMXBs or thermal-type spectra in general, their contribution to the CXB potentially could have a significant influence on AGN models of the CXB. On the other hand, if the LLNAS spectra extend out to ~ 40–50 keV without a spectral break, they they should, for the sole purpose of evaluating their CXB contribution, be treated as another class of AGNs at the low end of luminosity function since the relevant portion of their X-ray spectra would then not be different from AGN spectra in any fundamental way (in some cases, there may be genuine misclassifications). Only the distribution in spectral slopes may be different, but we note that AGNs contributing to the CXB (quasars, Seyfert 1 and Seyfert 2 galaxies) already represent a wide range of slopes (see, e.g., Turner & Pounds 1989; Williams et al. 1992; Nandra & Pounds 1994). Sensitive hard-X-ray observations are required to determine whether the ~ 10–50 keV spectra exhibit significant deviations from a power law, as do those of Seyfert 1 galaxies (see, e.g., Nandra & Pounds 1994).

The authors wish to thank M. Dahlem, T. Heckman, and G. Fabbiano for their contribution to this work and making their *ROSAT* results available prior to publication. We thank Keith Gendreau for many useful discussions. We also thank the operations staff at ISAS, who made this and many other *ASCA* observations possible. This research made use of the HEASARC on-line service provided by NASA/GSFC. An anonymous referee is thanked for making some useful suggestions.

REFERENCES

Bhattacharya, D., et al. 1994, ApJ, 436, 173
Boldt, E. 1987, Phys. Rep., 146, 215
Boyle, B. J., Griffiths, R. E., Shanks, T., Steward, G. C., & Georgantopoulos, I. 1993, MNRAS, 260, 49
Boyle, B. J., Shanks, T., Georgantopoulos, I., Stewart, G. C., & Griffiths, R. E. 1994, MNRAS, 271, 639
Bregman, J. N., & Glassgold, A. E. 1982, ApJ, 263, 564
Comastri, A., Setti, G., Zamorani, G., & Hasinger, G. 1995, A&A, 296, 1
Dahlem, M., Heckman, T. M., & Fabbiano, G. 1995, ApJ, 442, L49
Fabbiano, G., Heckman, T., & Keel, W. C. 1990, ApJ, 355, 442
Gendreau, K. C. 1994, *ASCA* Newsl., No. 2, 5
———. 1994, in New Horizon of X-Ray Astronomy, ed. F. Makino & T. Ohashi (Tokyo: Universal Acad. Press), 365
Griffiths, R. E., & Padovani, P. 1990, ApJ, 360, 483
Gruber, D. A. 1992, in The X-Ray Background, ed. X. Barcons & A. C. Fabian (Cambridge: Cambridge Univ. Press), 44
Hartmann, D., & Burton, W. B. 1995, in The Leiden-Dwingeloo Atlas of Galactic Neutral Hydrogen (Cambridge: Cambridge Univ. Press), in press
Hasinger, G., Burg, R., Giaconni, R., Hartner, G., Schmidt, M., Trümper, J., & Zamorani, G. 1993, A&A, 275, 1
Iwasawa, K., Yaqoob, T., Awaki, H., & Ogasaka, Y. 1994, PASJ, 46, L167
Jones, L. R., et al. 1995, in Wide-Field Spectroscopy and the Distant Universe, ed. S. Maddox & A. Aragón-Salamanca (Singapore: World Sci.), in press
Kim, D.-W., Fabbiano, G., & Trinchieri, G. 1992, ApJS, 393, 134
Kubo, H., Ikebe, Y., Makishima, K., & the GIS Team. 1994, *ASCA* Newsl., No. 2, 14
Madau, P., Ghisellini, G., & Fabian, A. C. 1993, ApJ, 410, L7
———. 1994, MNRAS, 270, L17
Makishima, K. 1994, in New Horizon of X-Ray Astronomy, ed. F. Makino & T. Ohashi (Tokyo: Universal Acad. Press), 171
Makishima, K., Ohashi, T., Kondo, H., Palumbo, G. G. C., & Trinchieri, G. 1990, ApJ, 365, 159
Makishima, K., et al. 1994, PASJ, 46, L77
Matt, G., & Fabian, A. C. 1994, MNRAS, 267, 187
Mitsuda, K., et al. 1984, PASJ, 36, 741
Miyaji, T., Lahav, O., Jahoda, K., & Boldt, E. 1994, ApJ, 434, 424
Moran, E. C., Halpern, J. P., & Helfand, D. J. 1994, ApJ, 433, L65
Nagase, F. 1989, PASJ, 41, 1
Nandra, K., & Pounds, K. A. 1994, MNRAS, 268, 405
Ohashi, T., Makishima, K., Tsuru, T., Takano, S., Koyama, K., & Stewart, G. C. 1990, ApJ, 365, 180
Ohashi, T., & Tsuru, T. 1992, in Frontiers of X-Ray Astronomy, ed. Y. Tanaka & K. Koyama (Tokyo: Universal Acad. Press), 435
Okada, K., Mihara, T., & Makishima, K., & the *ASCA* Team. 1994, in New Horizon of X-Ray Astronomy, ed. F. Makino & T. Ohashi (Tokyo: Universal Acad. Press), 515
Petre, R. 1993, in The Nearest Active Galaxies, ed. J. Beckman, L. Colina, & H. Netzer (Madrid: CSIC), 117
Petre, R., Mushotzky, R. F., Serlemitsos, P. J., Jahoda, K., & Marshall, F. E. 1993, ApJ, 418, 644
Petre, R., Okada, K., Mihara, T., Makishima, K., & Colbert, E. J. M. 1994, PASJ, 46, L115
Ptak, A., Yaqoob, T., Serlemitsos, P. J., Kunieda, H., & Terashima, Y. 1996, ApJ, in press
Rephaeli, Y., Gruber, D., & Persic, M. 1995, A&A, 300, 91
Ricker, P. M., & Mészáros, P. 1993, ApJ, 418, 49
Saunders, W., Rowan-Robinson, M., Lawrence, A., Efstathiou, G., Kaiser, N., Ellis, R. S., & Frenk, C. S. 1990, MNRAS, 242, 318
Setti, G., & Woltjer, L. 1989, A&A, 224, L21
Soifer, B. T., Sanders, D. B., Madore, B. F., Neugebauer, G., Danielson, G. E., Elias, J. H., Lonsdale, C. J., & Rice, W. 1987, ApJ, 320, 238
Takano, M., Mitsuda, K., Fukazawa, Y., & Nagase, F. 1994, ApJ, 436, L47
Tanaka, Y., Inoue, H., & Holt, S. S. 1994, PASJ, 46, L37
Turner, T. J., & Pounds, K. A. 1989, MNRAS, 240, 833
Warwick, R. S., Sembay, S., Yaqoob, T., Makishima, K., Ohashi, T., & Tashiro, M. 1993, MNRAS, 265, 412
Williams, O. R., et al. 1992, ApJ, 389, 157
Yaqoob, T., Ebisawa, K., & Mitsuda, K. 1993, MNRAS, 264, 411
Yaqoob, T., Serlemitsos, P. J., Mushotzky, R. F., Madejski, G., Turner, T. J., & Kunieda, H. 1994a, PASJ, 46, L173
Yaqoob, T., et al. 1994b, PASJ, 46, L49
Zdziarski, A. A., Johnson, N. W., Done, C., Smith, D., & McNaron-Brown, K. 1995, ApJ, 438, L63